

The Glass Transition of Water, Based on Hyperquenching Experiments

V. Velikov, S. Borick, C. A. Angell*

The glass transition temperature (T_g) in water is still uncertain, with conflicting values reported in the literature. As with other hyperquenched glasses, water exhibits a large relaxation exotherm on reheating at the normal rate of 10 kelvin (K) per minute. This release of heat indicates the transformation of a high enthalpy state to a lower one found in slow-cooled glasses. When the exotherm temperature is scaled by T_g , the good glass-formers show a common pattern. However, for hyperquenched water, when this analysis is performed using the commonly accepted $T_g = 136$ K, its behavior appears completely different, but this should not be the case because enthalpy relaxation is fundamental to the calorimetric glass transition. With $T_g = 165 \pm 5$ K, normal behavior is restored in comparison with other hyperquenched glasses and with the binary solution behavior of network-former systems (H_2O , ZnCl_2 , or BeF_2 plus a second component). This revised value has relevance to the understanding of water-biomolecule interactions.

The glassy state of water is the dominant form in the Universe (1). It is formed by the slow accumulation of water molecules from the vapor state onto cold substrates such as dust particles, which later agglomerate into the larger bodies we call comets. This vapor-deposited material, which can also be formed in the laboratory, has been called amorphous solid water (ASW) (2), the amorphous structure having been shown by the absence of crystalline x-ray peaks (3, 4). Because it has the appearance of a glass when carefully prepared, it was expected to have a glass transition temperature T_g at which molecular relaxation occurs on a time scale of minutes (5).

In a succession of studies since 1950 (6), the glass transition, as detected by more or less sudden increases in heat capacity during heating (5), has been either not found at all (6–8) or clearly seen (9, 10). A value of $T_g = 136$ K was finally assigned on the basis of both extrapolations of unambiguous glass transitions measured in binary aqueous solutions (7, 11, 12) and of a weak and broad thermal effect observed after extended annealing of the initial deposit at 130 K (13). The latter procedure was adopted and it proved capable of revealing a similar effect in a glassy form of water made directly from the liquid (14) by an aerosol droplet hyperquenching technique (15, 16). We investigate this form of vitreous water, known as hyperquenched glassy water (HQGW).

An alternative vitreous form, low-density amorphous water (LDAW), is obtained by

the high-pressure collapse of crystalline ices to high-density amorphous water followed by annealing at 100 K at ambient pressure (17). This form yielded $T_g = 124$ K for scans of 0.17 K/min (18) and 129 K at 30 K/min (19). Extended annealing above 136 K (20) did not remove these subtle differences between LDAW and HQGW, implying kinetic stability for two distinct liquid forms [waters A and B (20)].

Intrinsic to the notion of T_g for a substance is that, above this temperature, the substance is a viscous liquid for any measurement conducted on normal time scales (minutes). For LDAW, the assignment $T_g = 136$ K was affirmed by blunt probe dielectric penetrometry (21) in which the probe was found to penetrate the amorphous phase, but not ice, in the temperature range 140 to 150 K. The combination of such observations with the calorimetric findings has led to the wide adoption of $T_g = 136$ K for water (19, 22, 23).

However, contrary results were obtained from a falling ball nanoviscosimetry experiment (24, 25). Ions that had been soft-landed on a glassy film deposited on a metal substrate were observed to penetrate the film when their viscosities became liquid-like during heating. For well-known molecular glass-formers such as propanol and branched hydrocarbons, penetration was observed when the temperature was raised some 10% above the glass transition temperature [at which viscosities are about 10^{10} Pa·s (5)]. However, no penetration was observed for vitreous water (ASW) films up to the crystallization temperature at 155 K. This observation is consistent with results of isotopic scrambling experiments (26), which seem incompatible with water having viscous liquid

behavior, and thus center-of-mass diffusion, near 136 K.

These observations, and also the unexpected existence of two liquid waters A and B with minor differences in properties, would all be understandable if water's T_g , for measurements on normal time scales, were to lie above the crystallization temperature. Here we demonstrate that this is indeed the case by analyzing the original exothermic effects (27) in light of new measurements on hyperquenched molecular liquids and their correlation with similar observations on glassy metals and silicates.

The calorimetric results from the report of Hallbrucker and Mayer on the hyperquenched glass (27) are reproduced in Fig. 1. The release of heat started at 120 K and continued until crystallization commenced at 155 K. This release of heat was interpreted as the relaxation of the high-energy quenched state to a lower enthalpy state characteristic of slowly cooled glasses. Such enthalpy recovery exotherms are well known in the calorimetry of glasses that have been cooled at rates in excess of the reheating rate (28–30) and are particularly marked in the only well-studied case of a hyperquenched glass-former that does not crystallize on reheating (a standard soda-lime-silica glass) (31, 32). Their existence is predicted (30, 31, 33–35) even by very simple treatments (35).

To illustrate the effect of cooling rate and to provide comparisons between water and hyperquenched samples of a “good” glass-former (no crystallization upon heating), we studied the model molecular glass-former orthoterphenyl (OTP). In Fig. 2A, a “standard scan” for a sample in which the cooling and heating rates are the same ($-Q^S = +Q^S = 20$ K/min) is compared with one for which the cooling rate is the maximum permitted by our calorimetry instrument (PerkinElmer DSC-7), namely -247 K/min. Curve A in Fig. 2B shows the difference between the two. The area under curve A is a measure of the difference in their “frozen-in,” or excess, enthalpies resulting from the differences in their cooling rates. The much larger effect for a hyperquenched sample of OTP is shown by the dashed curve in Fig. 2B (see below).

The freezing-in temperature (i.e., the T_g during cooling) is often called the fictive temperature T_f . For the standard scan it can be assigned a precise value, T_f^S in Fig. 2A, from the heating curve by means of the Moynihan construction (28, 29). This replaces the curvilinear scan with a rectangular function such that energy is conserved.

The fictive temperature T_f^Q for any glass formed at a cooling rate Q different from that of the standard can be obtained from the excess enthalpy H_{ex} , distinguishing it from the standard glass (i.e., the areas under the Fig. 2B curves). For each case, this area is subtracted from the liquid branch of the standard scan of Fig. 2A to

Department of Chemistry and Biochemistry, Arizona State University, Tempe, AZ 85287, USA.

*To whom correspondence should be addressed. E-mail: caa@asu.edu

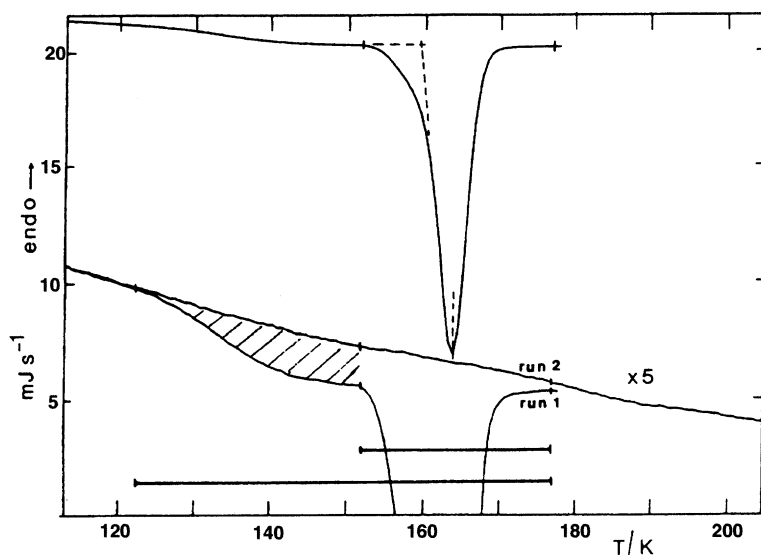


Fig. 1. Initial and second differential scanning calorimeter upscans of hyperquenched glassy water, showing (hatched area) the exothermic release of enthalpy stored in the hyperquenched state [adapted from (27)]. The second scan (after crystallization) serves as an event-free reference for the first (27).

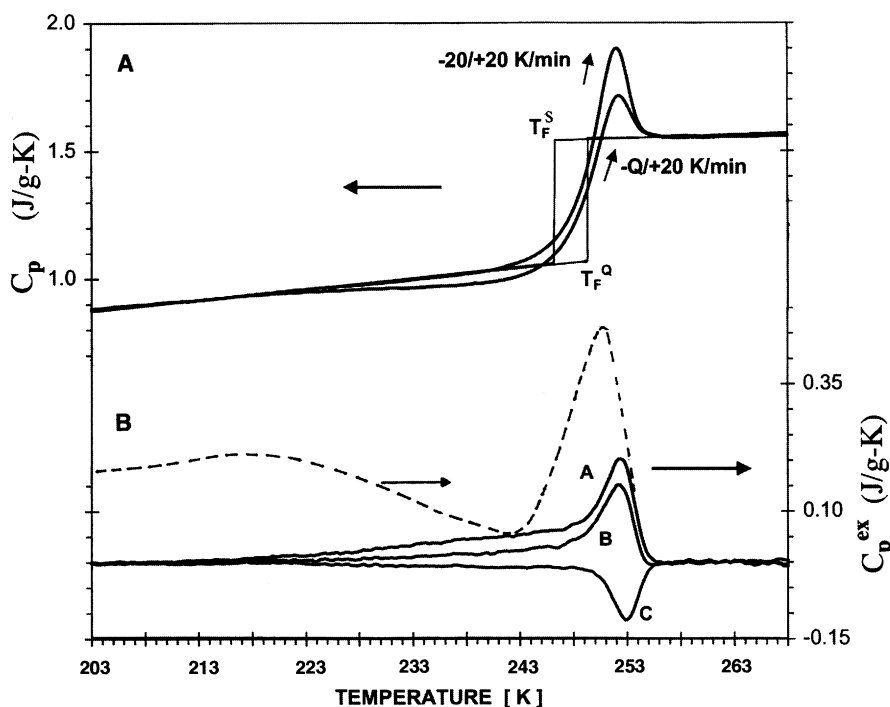


Fig. 2. (A) DSC upscans, at the "standard" heating rate $+Q^S$ of 20 K/min, of two OTP glasses formed at different cooling rates: (i) -20 K/min ($-Q^S$), and (ii) a rate $-Q$ K/min (-247 K/min). The upper scan is called the "standard scan." Step function defines fictive temperature of the standard scan, which coincides with the glass transition temperature defined by the " C_p onset" criterion (28, 29). The area between the scans is used to obtain the fictive temperature of the faster-cooled glass, T_F^Q . (B) Excess heat capacities $C_p^{\text{ex}} = C_p(\text{standard}) - C_p(\text{quenched})$ for nonstandard scans (solid curves): The difference between the two curves of (A) is shown as curve A. All heating rates are 20 K/min. Curve B is for a cooling rate of -73 K/min, and curve C is for -10 K/min. Their integrals are used to obtain the fictive temperatures (28, 29, 33). The dashed curve is the excess heat capacity obtained for the hyperquenched OTP sample, which was quenched at a rate some four orders of magnitude faster than any of the others (see text) and hence exhibits a much greater excess heat capacity (for complete exotherm, see Fig. 4). The excess heat capacity for hyperquenched glasses is also of different form, showing a maximum well below T_g (31).

satisfy $H_{\text{ex}} = \Delta C_p(T_F^Q - T_F^S)$, where ΔC_p is the jump in heat capacity at T_g and T_F^S is the fictive temperature for the standard scan. For the glass formed at the maximum instrument cooling rate, the fictive temperature found by this construction is marked T_F^Q in Fig. 2A, where Q is still to be determined.

To determine Q , we made a calibration plot (Fig. 3) using the T_F values determined from curves B and C in Fig. 2B. These are for known coolings, -73 K/min (fastest controlled cooling rate available) and -10 K/min, followed by standard heatings. The fictive temperatures and the cooling rates are scaled by the standard values.

Figure 3 is a modified version of the plot used by Moynihan (28, 29) to demonstrate that the activation energy for enthalpy relaxation is the same as that for viscosity. Our (scaled) plot yields a slope that, rather than being the activation energy, E_a , is the " m fragility" (36) of the liquid. It is related to E_a by

$$m = E_a / 2.303RT_g \quad (1)$$

(36), where T_g is now T_F of the standard scan. The m fragility obtained for OTP by the slope of Fig. 3 is 77, which is in excellent agreement with the value of 76 obtained from viscosity data (37) and with the value of 81 obtained from dielectric relaxation data (36).

We use Fig. 3, supported by viscosity data (37), to obtain the quenching rate of the hyperquenched OTP glass from its measured fictive temperature. This glass was made by quenching tiny electrospayed droplets (38) into a liquid nitrogen-cooled DSC pan. The large excess heat capacity then obtained upon upscanning at Q^S K/min (Fig. 2B) is similar to that found for the melt-spun silicate glasses (31, 32). The sharp peak near T_g is exaggerated in OTP because of its higher fragility. In addition to this feature for fragile systems, there is a maximum in the excess heat capacity located below the temperature of the normal glass transition. The fictive temperature found for the hyperquenched OTP glass (inset, Fig. 3) is high, $1.076T_F^S$ [although it is much higher for strong liquids quenched at the same rate (31)].

The calibration line shows that the effective cooling rate must have been 4×10^6 K/min. This is almost as high as that attributed to water (Fig. 1) when hyperquenched by the aerosol sput technique (15, 16) and thus affords a good basis for comparison. By contrast, the Fig. 2A DSC-quenched sample, $T_F = 1.014T_F^S$, yields $-Q$ of only 247 K/min, as expected from the manufacturer's description. This is not high enough to develop the broad maximum in C_p^{ex} .

Examination of upscan exotherms from cases of hyperquenched (melt-spun) metallic glasses shows similar exotherms with maximum excess heat capacities (39). This is also found in our study (38) of a melt-spun pitch (an aromatic hydrocarbon glass used as

REPORTS

graphite fiber precursor) for which the cooling rate is estimated to be 10^5 K/min (40, 41). The comparable results for silicate glasses hyperquenched by fiber-drawing to very small diameter (31) have already been referred to as the only previous case of a good glass-former studied after hyperquenching. In all cases studied, including this latter non-fragile liquid case, the excess heat capacity (or enthalpy recovery exotherm) has its peak well below T_g . Furthermore, the enthalpy has fully recovered before the temperature $1.1T_{g, \text{onset}}$ [i.e., the end of the transformation range of a strong glass-former (22, 31)] is reached. However, this is not the case for the water data shown in Fig. 1 if T_g is 136 K.

To highlight this point more clearly, we collected all these data into a master plot (Fig. 4) using a T_g -scaled temperature axis, and we included the data from Fig. 1 by using the generally accepted value for the glass transition temperature, 136 K (14–23). At T_g -scaled temperatures, where the other glasses have fully released the trapped-in enthalpy of the hyperquench and become viscous liquids, the glassy water structure is still slowly relaxing. Much of the excess heat capacity is still present when crystallization occurs at 155 K (Fig. 1).

From the data in Fig. 4 we should conclude that water, rather than being a fragile liquid near 150 K (42, 43) or even a strong liquid (22), is not a liquid at all (i.e., $T_g > 150$ K), in agreement with (24–26) and also (7). Indeed, such a conclusion is consistent with the report in (14) that the activation energy for structural relaxation is 55 kJ/mol, essentially the value found for diffusion of water molecules in ice. To avoid this conclusion, it would be necessary for water to have some additional source of slow enthalpy release that grafts smoothly onto the glassy relaxation in such a way as to produce the deviation from normal behavior observed in Fig. 4. This could conceivably be some effect of freezing of prenucleated droplets (44) or slow modes of a partially frozen cooperative transition (45, 46), but any such explanation must be coupled with an explanation as to why vitreous water, with $T_g = 136$ K, does not begin to release any frozen-in enthalpy until a reduced temperature much higher than for the other liquids of Fig. 4 is reached.

If the primary T_g is higher than 136 K and also above the crystallization temperature, can a T_g value be assigned at all? The excess C_p of water can be overlapped with the other curves of Fig. 4, particularly with the fragile OTP, if we assign $T_g = 165$ K (curve F). To within 5 K, this is also (i) the temperature of the glass transition observed for water in nanodroplet inclusions in hydrogels (47, 48), and (ii) the temperature predicted (46) for the glass transition from water viscosities ($\eta \approx 10^{12}$ Pa·s for network glasses at T_g) extrapolated below the crystallization temperature

using entropy-viscosity correlations (34).

With this revised T_g we need to explain two outstanding observations concerning water. The first is, of course, the weak thermal effect previously assumed to be the glass transition in the different amorphous waters, at 136 K in ASW and HQGW (20, 21) and 129 K in LDAH (19).

If it is not the primary glass transition, then it must be, as suggested in (26), the freezing-in of nondiffusive defects analogous to the Bjerrum defects that are responsible for dielectric relaxation in (crystalline) ice I_h . This sort of decoupled reorientation mechanism could also be responsible for the dielectric relaxation seen in

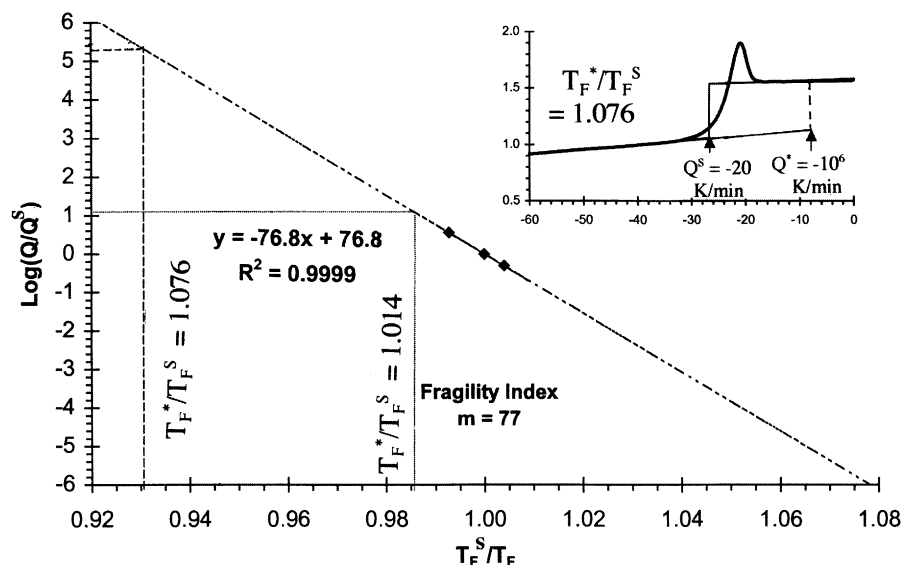


Fig. 3. Scaled Arrhenius plot of the cooling rates $-Q$ K/min versus the fictive temperatures of the resulting glasses. The scaling parameters are the standard cooling rate ($Q^S = -20$ K/min) and the fictive temperature T_F^S of the standard glass, formed by Q^S cooling. The slope of this plot is the m fragility index. The inset shows the matching of H_{ex} for the hyperquenched OTP glass (from Fig. 2B) to the standard scan to obtain T_F^* , which is then marked by the vertical dashed line to read off its quench rate.

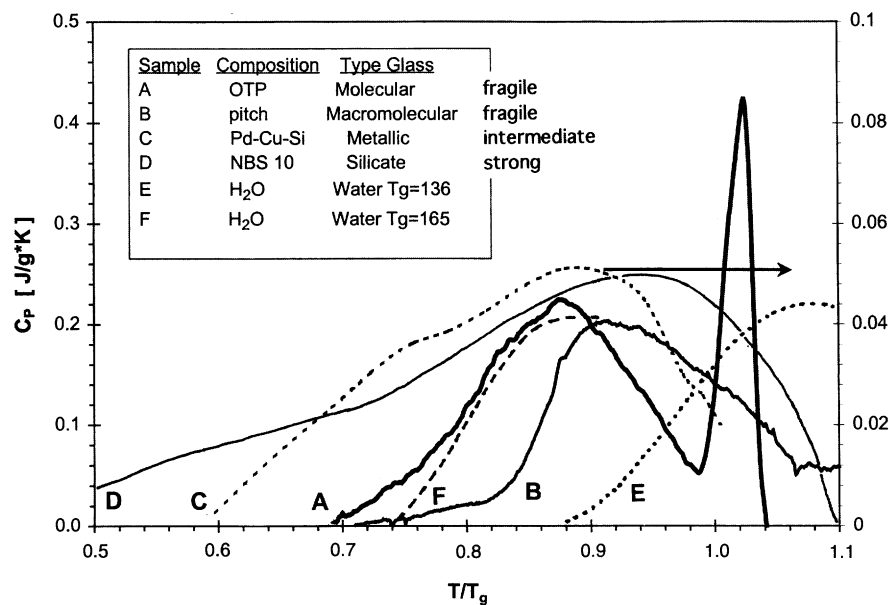


Fig. 4. Comparison of the excess heat capacities (enthalpy recovery exotherms) of various hyperquenched bulk glass-formers (38), with the excess heat capacity of hyperquenched water (Fig. 1), using a T_g -scaled temperature axis. The water data are plotted twice, first (dotted line, E) for $T_g = 136$ K (14), and second (dashed line F) for the choice $T_g = 165$ K. The bulk glass-formers, which range from "strong" (silicate) to "fragile" (OTP) in character, were all quenched at rates in the range 10^6 to 10^7 K/min. Note that in the observable supercooled state, water behaves as the most fragile of all liquids (22).

nanodroplet water imbibed in poly(2-hydroxyethyl-methacrylate) (polyHEMA) near its glass transition at 162 K [the value given for a 34 wt % water sample (47, 48)]. These dielectric relaxation times are also Arrhenius in character and faster than the relaxation responsible for the glass transition.

The second is the convergence of extrapolated binary solution T_g to the temperature 138 ± 2 K (7, 11, 12). Here the resolution must be (7) the recognition that aqueous binary system extrapolations are no more reliable than those of binary solutions of other network-formers such as SiO_2 , BeF_2 , and ZnCl_2 . In such solutions there are sudden drops of T_g with small additions of the second component as the tetrahedral network is disrupted. In recent studies (49) of the $\text{BeF}_2 + \text{LiF}$ system, for instance, the binary solution T_g data measured by DSC between 4 and 10 mol % LiF predict, by extrapolation, that the T_g for pure BeF_2 should be 394 K. However, the directly measured value for pure BeF_2 glass is very much higher, 590 K, according to both DSC (49) and viscosity (50) measurements. Because there is general agreement that glassy water is well described as a random tetrahedral network (51), the BeF_2 system data should suffice to show that earlier uses of binary system extrapolations to obtain T_g for water (11, 12) were not correct.

In light of the new assignment, the glass transitions observed in hydrated proteins (52, 53) take on a new aspect. T_g values in these systems are observed to decrease rapidly with increasing water content until they reach ~ 165 K, and then excess water crystallizes out as ice during cooling. Water in association with hydrophilic proteins behaves much like water in hydrogels (54). Both cases may reflect the behavior of water in the absence of crystallization.

Vitreous water, like most hyperquenched metallic glasses, apparently remains in the glassy state until it crystallizes (at 150 to 160 K). A possible exception is water sequestered in nanoscopic assemblages, which may play an important role in biophysical systems.

References and Notes

1. P. Jenniskens, S. F. Barnhak, D. F. Blake, M. R. S. McCoustra, *J. Chem. Phys.* **107**, 1232 (1997).
2. M. G. Sceats, S. A. Rice, in *Water: A Comprehensive Treatise*, F. Franks, Ed. (Plenum, London, 1982), vol. 7, pp. 83–211.
3. E. F. Burton, W. F. Oliver, *Nature* **135**, 505 (1935).
4. ———, *Proc. R. Soc. London Ser. A* **153**, 166 (1935).
5. C. A. Angell, *Science* **267**, 1924 (1995).
6. J. A. Pryde, G. O. Jones, *Nature* **170**, 635 (1952).
7. D. R. MacFarlane, C. A. Angell, *J. Phys. Chem.* **88**, 759 (1984).
8. J. A. Ghormley, *J. Chem. Phys.* **48**, 503 (1967).
9. J. A. MacMillan, S. C. Los, *J. Chem. Phys.* **42**, 829 (1965).
10. M. Sugisaki, H. Suga, S. Seki, *J. Chem. Soc. Jpn.* **41**, 2591 (1968).
11. C. A. Angell, J. C. Tucker, *J. Phys. Chem.* **84**, 268 (1980).
12. J. A. Ghormley, *J. Am. Chem. Soc.* **79**, 1862 (1957).
13. A. Hallbrucker, E. Mayer, G. P. Johari, *J. Phys. Chem.* **93**, 4986 (1989).

14. G. P. Johari, A. Hallbrucker, E. Mayer, *Nature* **330**, 552 (1987).
15. E. Mayer, *J. Appl. Phys.* **58**, 663 (1985).
16. ———, *J. Microsc.* **140**, 3 (1985).
17. O. Mishima, L. D. Calvert, E. Whalley, *Nature* **314**, 76 (1985).
18. D. D. Klug, Y. P. Handa, *J. Phys. Chem.* **92**, 3323 (1988).
19. A. Hallbrucker, E. Mayer, G. P. Johari, *J. Phys. Chem.* **93**, 7751 (1989).
20. G. P. Johari, A. Hallbrucker, E. Mayer, *Science* **273**, 90 (1996).
21. G. P. Johari, *J. Phys. Chem. B* **102**, 4711 (1998).
22. K. Ito, C. T. Moynihan, C. A. Angell, *Nature* **398**, 492 (1999).
23. O. Mishima, H. E. Stanley, *Nature* **396**, 329 (1998).
24. A. A. Tsekouras, M. J. Iedema, J. P. Cowin, *Phys. Rev. Lett.* **80**, 5798 (1998).
25. ———, in preparation.
26. M. Fisher, J. P. Devlin, *J. Phys. Chem.* **99**, 11584 (1995).
27. A. Hallbrucker, E. Mayer, *J. Phys. Chem.* **91**, 503 (1987).
28. C. T. Moynihan, A. J. Easteal, M. A. DeBolt, J. Tucker, *J. Am. Ceram. Soc.* **59**, 12 (1976).
29. ———, *J. Am. Ceram. Soc.* **59**, 16 (1976).
30. G. W. Scherer, *Relaxation in Glass and Composites* (Wiley, New York, 1986).
31. J. Huang, P. K. Gupta, *J. Non-Cryst. Solids* **151**, 175 (1992).
32. Y. Yue, in preparation. This study is of a nonstandard basalt glass, but is very detailed.
33. I. M. Hodge, *J. Non-Cryst. Solids* **169**, 211 (1994).
34. G. Adam, J. H. Gibbs, *J. Chem. Phys.* **43**, 139 (1965).
35. C. T. Moynihan, P. B. Macedo, *J. Phys. Chem.* **75**, 3379 (1971).
36. R. Bohmer, K. L. Ngai, C. A. Angell, D. J. Plazek, *J. Chem. Phys.* **99**, 4201 (1993).
37. W. T. Laughlin, D. R. Uhlmann, *J. Phys. Chem.* **76**, 2317 (1972).
38. V. Velikov, S. Borick, C. A. Angell, *J. Phys. Chem.*, in press.
39. H. S. Chen, E. Coleman, *Appl. Phys. Lett.* **28**, 245 (1976).
40. J. Doshi, D. H. Reneker, *J. Electrostat.* **35**, 151 (1995).
41. D. H. Reneker, I. Chun, *Nanotechnology* **7**, 216 (1996).
42. R. S. Smith, B. D. Kay, *Nature* **398**, 788 (1999).
43. D. Kivelson, G. Tarjus, *J. Phys. Chem. B* **105**, 6620 (2001).
44. E. Mayer, personal communication.
45. C. Meingast, F. Gugenberger, *Mod. Phys. Lett. B* **7**, 1703 (1993).
46. F. Starr, C. A. Angell, H. E. Stanley, in preparation.
47. K. Hofer, E. Mayer, G. P. Johari, *J. Phys. Chem.* **94**, 2689 (1990).
48. ———, *J. Phys. Chem.* **95**, 7100 (1991).
49. Zh. V. Dobrokhotova, B. S. Zakharova, *Inorg. Mater.* **36**, 191 (2000) (translated from the Russian original).
50. S. V. Nemilov, G. T. Petrovskii, L. A. Krylova, *Inorg. Mater.* **4**, 1453 (1968).
51. A. H. Narten, C. G. Venkatesh, S. A. Rice, *J. Chem. Phys.* **64**, 1106 (1976).
52. G. Sartor, E. Mayer, G. P. Johari, *Biophys. J.* **66**, 249 (1994).
53. J. L. Green, J. Fan, C. A. Angell, *J. Phys. Chem.* **98**, 13780 (1994).
54. G. Sartor, A. Hallbrucker, E. Mayer, *Biophys. J.* **69**, 2679 (1995).
55. R. J. Speedy, unpublished data.
56. Supported by NSF Solid State Chemistry Program grants DMR-9614531 and DMR-0082535. We acknowledge R. J. Speedy (55), who argued, using data from some of the same references cited here, that T_g should lie far above 136 K, perhaps near 220 K. We thank E. Mayer for sharing unpublished data.

19 April 2001; accepted 26 October 2001

High Geothermal Heat Flow, Basal Melt, and the Origin of Rapid Ice Flow in Central Greenland

Mark Fahnestock,¹ Waleed Abdalati,² Ian Joughin,³ John Brozena,⁴ Prasad Gogineni⁵

Age-depth relations from internal layering reveal a large region of rapid basal melting in Greenland. Melt is localized at the onset of rapid ice flow in the large ice stream that drains north off the summit dome and other areas in the northeast quadrant of the ice sheet. Locally, high melt rates indicate geothermal fluxes 15 to 30 times continental background. The southern limit of melt coincides with magnetic anomalies and topography that suggest a volcanic origin.

Basal melt and meltwater exert a strong influence on ice flow (1–4). Our limited knowledge of basal melt is derived from models and sparse observations of bed properties (5–

7). Here we introduce a technique that allows us to determine the extent and rate of basal melting for a large portion of the Greenland Ice Sheet using data from airborne ice-penetrating radar, and we relate that melting to ice flow patterns in the interior.

Radar soundings reveal internal layering (8–11) largely due to changes in electrical conductivity from inhomogeneous impurity concentrations within the ice. The impurities (e.g., dust from volcanic eruptions) are introduced from the atmosphere, forming layers

¹Earth System Science Interdisciplinary Center, University of Maryland, College Park, MD 20742, USA. ²NASA Headquarters, Washington, DC 20546, USA. ³Jet Propulsion Laboratory, Mail Stop 300-235, 4800 Oak Grove Drive, Pasadena, CA 91109, USA. ⁴Naval Research Laboratory, Washington, DC 20375, USA. ⁵Remote Sensing Laboratory, University of Kansas, Lawrence, KS 66045, USA.